

PCCP

Physical Chemistry Chemical Physics

Accepted Manuscript



This is an Accepted Manuscript, which has been through the Royal Society of Chemistry peer review process and has been accepted for publication.

Accepted Manuscripts are published online shortly after acceptance, before technical editing, formatting and proof reading. Using this free service, authors can make their results available to the community, in citable form, before we publish the edited article. We will replace this Accepted Manuscript with the edited and formatted Advance Article as soon as it is available.

You can find more information about Accepted Manuscripts in the [Information for Authors](#).

Please note that technical editing may introduce minor changes to the text and/or graphics, which may alter content. The journal's standard [Terms & Conditions](#) and the [Ethical guidelines](#) still apply. In no event shall the Royal Society of Chemistry be held responsible for any errors or omissions in this Accepted Manuscript or any consequences arising from the use of any information it contains.

ARTICLE

Using Ion-Selective Membranes to Study Cation Transport in Hybrid Organic-Inorganic Perovskite

Emily C. Smith^a, Christie L.C. Ellis^a, Hamza Javaid^a, Blaise G. Arden^a, D. Venkataraman^{a†*}

Received 00th January 20xx,
Accepted 00th January 20xx

DOI: 10.1039/x0xx00000x

Using a methylammonium selective membrane in conjunction with electrochemical impedance spectroscopy, we measured ion migration in methylammonium lead triiodide (MAPbI₃) with a millisecond (ms) time constant under illumination. These values are consistent with reported values of ionic conduction in thin-film perovskite solar cells. We monitored an electrochemical impedance response arising from ionic conductivity through MAPbI₃ and a methylammonium selective layer. We fit this complex impedance response to an intuitive circuit model which revealed an ionic species moving on a ms time scale. Electrospray ionization mass spectrometry (ESI-MS) reveals direct chemical evidence of methylammonium diffusion into the ion selective layer. We found no experimental evidence indicating the mobility of lead ions or protons, indicating that the mobile species observed under illumination is likely methylammonium.

A. Introduction

Ion transport—a central feature of Hybrid Organic-Inorganic Perovskite (HOIP) photovoltaics—affects many HOIP properties such as device stability, power conversion efficiencies (PCE), and hysteresis in current density (J)-voltage (V) curves.¹⁻⁵ Despite the importance of mobile ions in HOIPs, the chemical identity of the mobile ion is still under debate. In HOIPs it is likely that more than one mobile ion is responsible for the experimental observations of ion transport.⁶⁻⁸ In the most commonly studied HOIP, (CH₃NH₃)PbI₃ there are four possible mobile ions: H⁺, CH₃NH₃⁺ (MA⁺), Pb²⁺ and I⁻.⁶ Moreover, light and electrical bias can and do influence ion transport, but their impact on each ion may differ. With multiple possibilities for mobile ions, the influence of solar cell operating conditions on ion mobility, and coupled charge transport, studying ion transport in these materials has not been straightforward. Methods such as pulse-field gradient NMR that can be used to identify the mobile ion chemically are difficult to run *in-operando* (i.e., under device relevant conditions such as under light, heat and applied bias), whereas methods that are convenient to study ion transport *in-operando*, such as electrochemical impedance spectroscopy (EIS), lack chemical identity. These factors have led to diversity in opinion on the nature of ion transport in HOIPs. For example, in thin-film HOIP photovoltaics with a p-i-n device architecture, we observed evidence of ion transport using EIS and calculated an activation energy for the mobile ion in MAPbI₃ of 0.58 eV, which we attributed to MA⁺ migration. In a separate work, another group

found the same activation energy barrier of 0.58 eV, extrapolated from transient photovoltage decay measurements, but the value was attributed it to I⁻ vacancy migration.⁹ Understanding the nature and timescale of mobile ions is integral to fundamentally understanding photovoltaic device performance and engineering new devices with improved stability. Additionally, a comprehensive knowledge of the nature of ion transport in the material will allow us to take advantage of the mixed ionic-electronic transport for various iontronic applications such as electrochemical transistors and memristors for neuromorphic computing. Thus, it is imperative that we determine ways to selectively study ion transport in these materials.

One technique that is widely used to probe ion transport in mixed ionic-electronic conductors is electrochemical impedance spectroscopy (EIS).¹⁰⁻¹² EIS allows separation of charge and mass transport processes that occur on different time scales, making it ideal for separating electronic and ionic processes in HOIPs. From an EIS response, we can quantify kinetic parameters such as diffusion constant and activation energy barriers of ion transport.¹³ One important feature of EIS is that it can be used to study HOIP devices *in-operando* to obtain critical information about device operational parameters on the electronic and ionic transport. A missing feature in an EIS response is the determination of ionic chemical identity. As a result, we can associate features in EIS to an ionic process; however, we cannot conclusively relate those features with a particular ion. Thus, for HOIPs, where there is a possibility of more than one mobile ion, we raise the question: which ion is responsible for the EIS features associated with ion transport? We hypothesized that placing an ion-selective membrane between the active layer and the electrode would allow us to associate features in EIS with the selected ion. We reasoned that if we place an ion-selective membrane between the active layer and the electrode, then the membrane will selectively

^a Department of Chemistry, University of Massachusetts Amherst, Amherst Massachusetts 01003-9303, United States

† Corresponding author email: dv@chem.umass.edu

Electronic Supplementary Information (ESI) available: See DOI: 10.1039/x0xx00000x

allow one ion to reach the electrode, resulting in a primary EIS response from that ion. If we can attach chemical information to EIS data—the missing piece—we can selectively and quantitatively study each mobile ion in HOIPs under device relevant conditions.

Herein, using a polymer ion-selective membrane (ISM) that is selective for methylammonium ion (MA^+), we study the cationic transport in pristine methylammonium lead iodide (MAPbI_3) under illumination. We observed an EIS response consistent with ion transport through the material. Chemical characterization of the membrane using electrospray ionization mass spectrometry (ESI-MS) showed the presence of MA^+ in these membranes. We observe no evidence that the response arises from mobile Pb^{2+} or H^+ . Furthermore, we observe negligible I^- incorporation into the membranes in the solid-state. When we fit the EIS response to an equivalent circuit model, we find that ion transport occurs in our device on the millisecond timescale—the same timescale commonly observed in EIS of thin-film photovoltaic devices—that is consistent with a mobile MA^+ ion.

B. Experimental

HOIP Powder

MAPbI_3 powder was prepared as follows. A clean, dry 25 mL Erlenmeyer flask was charged with PbI_2 (552 mg, 1.19 mmol, Sigma Aldrich) and methylammonium iodide (202 mg, 1.27 mmol, GreatCell Solar) along with a stir bar. To the vial was added γ -butyrolactone (4 mL, Sigma Aldrich) and the solution was ultrasonicated until all components were visibly solvated. The solution was stirred while dichloromethane (DCM, 8 mL, dried over magnesium sulfate anhydrous), was added dropwise. After the addition of DCM, stirring was removed, and a black precipitate was allowed to settle for 1 h before collection into two centrifuge tubes. The precipitate-containing solutions were centrifuged at 3500 rpm for 35 s or until the precipitate was fully sedimented. The remaining liquid was discarded, and the tubes containing precipitate were filled with fresh DCM (10 mL). Each tube was ultrasonicated until the black powder was resuspended in solution and centrifuged again at 3500 rpm for 35 s. The liquid was discarded. The powder was washed with DCM in this manner twice more. The powder was air dried for ~ 1 h and annealed at 100 °C for 1 h. The resulting MAPbI_3 powder (732 mg, 1.18 mmol, 99%) was stored in a vacuum oven overnight before further use. Powder x-ray diffraction (XRD) shows MAPbI_3 in the tetragonal phase and indicates no evidence of incomplete conversion from PbI_2 (Figure S1)

Ion Selective Electrodes

ITO coated glass substrates (1.5 cm x 1.5 cm, $\sim 20 \Omega \text{ sq}^{-1}$) were cleaned by ultrasonication of the substrates submerged in soap and water, then DI water, then acetone, then isopropyl alcohol for 20 min each. Some ITO substrates were reused after testing

to conserve resources. In the case of reuse, the substrates were first rinsed with tetrahydrofuran then ultrasonicated with dichloromethane before cleaning by the procedure above. The cleaned substrates were dried in an oven at 140 °C for at least 2 h before use. Methylammonium selective membranes were prepared as follows. To a clean, dry vial was added polyvinylchloride (30 mg, 0.71 inherent viscosity, Acros Organics), dibenzo-18-crown-6 (2 mg, 5.5 μmol , Avacado Research Chemicals Ltd.), Bis(2-ethylhexyl)phthalate (DEHP) (110 μL , Sigma Aldrich) and tetrahydrofuran (1 mL, dried over 3 Å activated molecular sieves). The components were ultrasonicated until solids fully dissolved. The solution was filtered through a 0.45 μm polytetrafluoroethylene (PTFE) filter (Restek). The membrane solution was drop cast onto cleaned ITO substrates (100 μL) then left to dry overnight before use.

HOIP Pellets

Pellets of MAPbI_3 were prepared as follows. The MAPbI_3 powder was ground finely in a mortar and pestle lined with clean weigh paper. Pellets were hand-pressed with a conventional KBr pellet press (International Crystal Laboratories) using ~ 70 mg of powder. Pellet dimensions were reproducible with this method; 7 mm diameter and ~ 0.5 - 0.6 mm thickness (measured by a digital micrometer).

Impedance Device Architecture

To make a device for impedance analysis, a MAPbI_3 pellet was sandwiched between two ion-selective electrodes in a staggered conformation so that some of the ITO coated portions of each substrate was accessible for clips during sample measurements. This configuration was compressed by clipping the sample with two $\frac{3}{4}$ in. mini spring clamps. A picture of a real device can be found in Figure S2.

Methylation of poly(4-vinylpyridine)

To a 50 mL round bottom flask was added poly(4-vinylpyridine) ($\sim 50,000$ kDa, 2.5 g), iodomethane (1.41 mL, 22 mmol), and distilled water (20 mL). The reaction mixture was sonicated for 1 h or until solids had dissolved. The dark yellow solution was concentrated and precipitated in acetone to yield a yellow powder (1.48 g). The product was verified by IR where characteristic quaternary ammonium bends were observed at 1639 cm^{-1} and 1187 cm^{-1} (Figure S3). For clear impedance results, the product was not dried before testing to allow small amounts of water to act as a plasticizer, boosting ion transport. The impedance response of the product after drying under vacuum overnight shows some signs of ion transport; however, the resistance is much higher in the dry sample, which led to results with significant noise making it difficult to analyze.

Mass Spectrometry Samples

Membrane devices were prepared as described above, using 40 μL of DEHP. The device was biased at ~ 1.5 V for 12 h using a standard AA battery attached to each ITO substrate via electrical leads. At the conclusion of the experiment, the HOIP sample was removed from the membranes. The surface of the membranes were rinsed with DMF until it ran clear (~ 0.5 mL).

The membranes were then dissolved in DCM which was subsequently evaporated via a gentle stream of air at 60 °C. The membrane powder was sonicated in 0.5 mL millipore water for 2 h. The water solution was filtered through a 0.2 μm polyethersulfone filter. ESI-MS was obtained on the solution in both positive and negative mode.

Characterization

Impedance spectroscopy was performed as a 2-point measurement using a Solartron Analytical SI 1287 Electrochemical Interface with a 1252A Frequency response analyzer. Samples were kept at rt in ambient atmosphere during measurements. Samples were illuminated with a 100 W incandescent light during measurement. AC conductivity was measured in a through-plane configuration from 300,000 – 0.1 Hz at an AC amplitude of 100 mV. DC bias was applied while holding the bottom electrode as a reference to zero any intrinsic parasitic voltage due to imperfect electrodes. Resulting Nyquist plots were modeled and fitted using ZView software (Scribner Associates).

Powder X-Ray diffraction (XRD) was taken in a Bragg-Brentano configuration using a Rigaku SmartLab SE X-ray diffractometer with a D'tex 250 Ultra ID Si strip detector. Measurements were taken from $2\theta = 10^\circ$ to 40° with a Cu K_α (1.542 Å) x-ray source. Mass analysis was obtained using a Bruker AmaZon ETD quadrupole ion trap mass spectrometer with an electrospray ionization source. The capillary voltage was held at 4.5 kV, and samples were directly injected at a flow rate of 4 $\mu\text{L}/\text{min}$. The acquisition time for each sample was ~ 2 min.

FTIR experiments were run using a Bruker Alpha-P equipped with an attenuated total reflectance (ATR) platinum diamond optic. Spectra were obtained between 4000 and 375 cm^{-1} with a resolution of 4 cm^{-1} .

Elemental mapping of the membranes was carried out using a Magellan 400 L XHR-SEM equipped with an Oxford X-MAX 80mm² Energy Dispersive X-ray Spectrometer. The beam acceleration voltage and current were set to 30 kV and 100 pA respectively. Spectra were obtained up to 20 keV. Wide sample areas of ~ 500 μm were analyzed.

C. Results and Discussion

Electrochemical Impedance Spectroscopy

In EIS, we can probe materials with non-linear current (I) – voltage (V) relationships. This technique applies an AC applied voltage and measures a resulting AC current. The use of a sinusoidal voltage allows us to sweep variable frequencies. Therefore, we can probe conduction processes that occur on a fast (high-frequency) or slow (low-frequency) timescale. The resulting sinusoidal response can be separated into its real and imaginary components and plotted in a complex plane. In EIS, this representation is called a Nyquist plot (Figure 1b). The shape of the Nyquist plot gives us insight into the physical processes occurring within the system. Most simple electronic semiconductors appear as a single semi-circle in the Nyquist

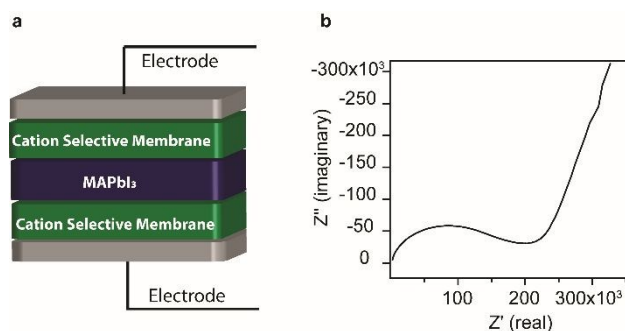


Figure 1. (a) An example device schematic. The electrodes are indium tin oxide (ITO) coated glass. The ITO substrates were coated with a cation selective ISM. A pellet of HOIP powder was sandwiched between two ion-selective electrodes, and the device was held together with spring-loaded clamps. (b) The EIS response from the device in (a).

plot. The appearance of additional features indicates the presence of unique conduction processes. High-frequency data points corresponding to faster-timescale conduction processes are represented on the left most side of the plot (closest to the origin), while low-frequency data points corresponding to slower-timescale processes represented by data on the right side. With this information, we can model the EIS response to determine specific values for various physical processes.

Ion-Selective Membrane Conductivity

A schematic of our devices is shown in Figure 1a. We employed an ion selective membrane (ISM) containing polyvinyl chloride (PVC) as an electronically insulating material, bis(2-ethylhexyl)phthalate (DEHP) as a membrane solvent, and dibenzo-18-crown-6 (DB18C6) as a cation-selective ionophore (see chemical structures in Figure S4). We chose this membrane because of its high selectivity for MA^+ ions and it displays near-Nernstian behavior for ions in solution.¹⁴⁻¹⁷

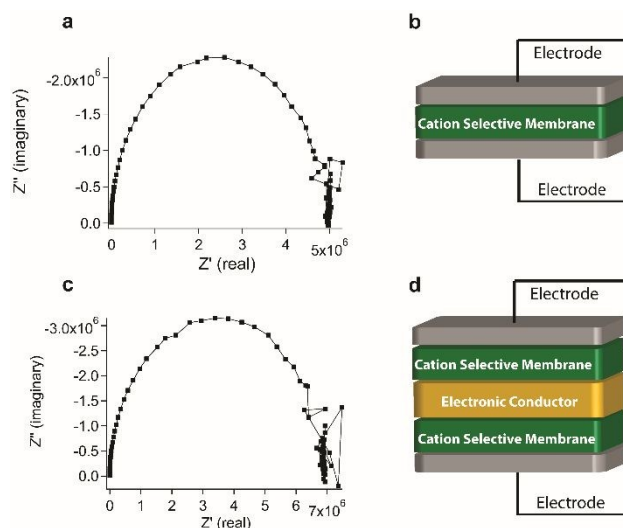


Figure 2. (a) EIS response of a sample set up as shown in (b). This complex EIS response has been observed before in PVC membranes containing plasticizer and depicts a relaxation of dipoles. (b) a schematic of the device from (a). (c) EIS response of a sample set up as shown in (d). We observe no new features eluding to electronic conduction through the ISM.

First, we measured the impedance response of a pristine ISM sandwiched between two ITO-coated substrates (Figure

2a,b). We saw a response extending into low frequencies that is characteristic of an electronically insulating dielectric material and has been observed for plasticized PVC membranes.¹⁸ Due to the thickness of the HOIP pellets (~mm), and the electronically insulating nature of the ISM, we expect minimal contribution from electronic charge carriers in the response of the full device. To verify this, we measured the EIS response of a conductive bronze plate sandwiched between two ISM-coated electrodes (Figure 2c,d). We expected to see new features in the high-frequency region of the Nyquist plot if there was a significant electronic contribution. However, the EIS response of bronze plates sandwiched between two ISM-coated electrodes was similar to that of the pristine ISMs, indicating that there is no electronic contribution from the membranes, as expected.

Having established that the ISMs are electronically-blocking, we then used ISM-coated electrodes to measure the EIS response of a pellet of MAPbI₃ under illumination (see supporting information Figure S5 and Figure S6 for EIS response of pristine MAPbI₃, and the ISM device under dark conditions). The EIS response of this device is shown as a Nyquist plot in Figure 1b. We observed new features in the Nyquist plot, which was absent in EIS responses of pristine ISM and the bronze plate-ISM controls. As the ISMs are electronically blocking, we attributed this new response to ionic conductivity within the HOIP sample. We also considered an alternate possibility that this response might arise from MA⁺ ions adsorbed into the ISM at the ISM-HOIP interface. We, therefore, examined the EIS responses of pellets of methylammonium iodide (MAI) and lead iodide (PbI₂) sandwiched between ISM electrodes. Both these materials are poor ionic conductors. In both samples, there were no EIS responses, consistent with poor ionic conductivity. Based on these results, we discounted the possibility that adsorbed MA⁺ ion at the ISM-HOIP interface is the cause of EIS response we observe in our ISM devices.

ISM Chemical Characterization

Having established that we are selectively seeing ionic response in the EIS of our ISM-HOIP devices, we then characterized the ISM to establish the chemical identity of the mobile ion. Since we chose the ISM to be selective for MA⁺, we expected to see chemical signatures of MA⁺ in the ISM after experimentation. To test this, we sandwiched a HOIP pellet between two ISM coated electrodes and applied a bias of 1.5 V under illumination for 12 h. We carefully peeled the HOIP pellet from the ISM. Chemical analysis of the resulting membranes with Fourier transform infrared spectroscopy (FTIR) showed evidence of MA⁺ incorporated into the ISM characterized by N-H and C-H bend absorptions between 1500-1600 cm⁻¹ and 1490 cm⁻¹, respectively (Figure S7).¹⁹ However, we note that the pristine ionophore, DB18C6, also absorbs in this region so this result is not conclusive for MA⁺. We then conducted an identical experiment, but after peeling away the HOIP pellet, we rinsed the surface of the ISM with dimethylformamide (DMF) to remove any excess HOIP material stuck to the ISM after experimentation. We analyzed the chemical composition of the remaining membrane material in solution using ESI-MS (Figure

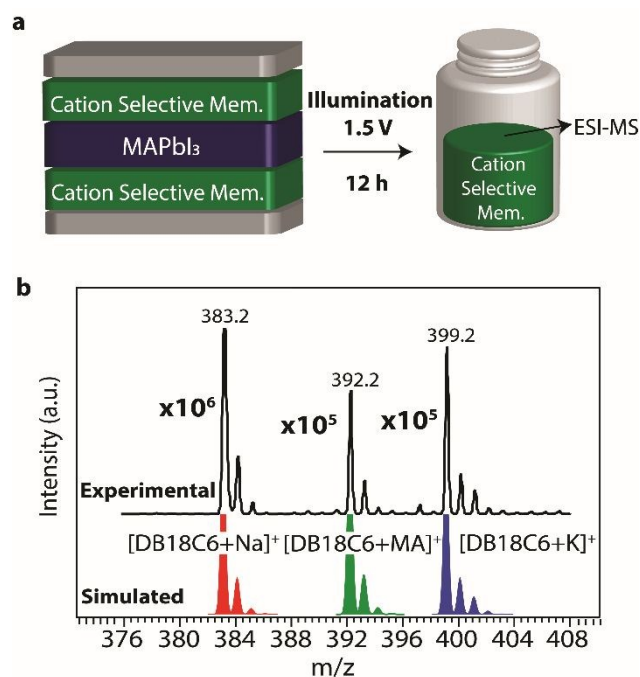


Figure 3. (a) Schematic of ESI-MS experimental conditions (b) ESI-MS spectrum obtained in positive mode of the membranes after the experiment. Peaks are observed corresponding to DB18C6 complexed to MA⁺, Na⁺, and K⁺ as illustrated by the simulated spectra for these charged complexes.

3). We observed characteristic peaks corresponding to DB18C6 complexed to MA⁺ at 392.2 m/z, consistent with the monoisotopic mass and isotopic distribution of this species. We additionally observed DB18C6 complexes with Na⁺ and K⁺ at 383.2 and 399.2, respectively. DB18C6 readily complexes both Na⁺ and K⁺. Thus, these peaks were anticipated and likely represent ambient impurity during the experimental workup. We did not observe characteristic peaks associated with Pb²⁺ or I⁻ (in the negative ion mode) of free ions or ions complexed to DB18C6 in ESI-MS (Figure 4). Since the binding constant (logK_b) for ammonium cations and Pb²⁺ are similar with respects to DB18C6 (2.94 and 5.05 respectively, measured by polarography),²⁰ simple diffusion of MA⁺ into the membrane cannot account for the appearance of this species, since we would expect similar diffusion of Pb²⁺ ions. This observation also confirms that the observed MA⁺ peak is not from excess HOIP sample stuck on the membranes after the DMF wash step. Energy dispersive x-ray analysis (EDX) of the membranes after exposure to the HOIP sample showed EDX peaks at energy values associated with iodine that is barely discernible from the baseline noise (Figure S8). Thus, we conclude I⁻ may be present in the ISM at concentrations at or below the detection limit of the instrument (1000 ppm), which does not represent a significant contribution when compared to MA⁺.

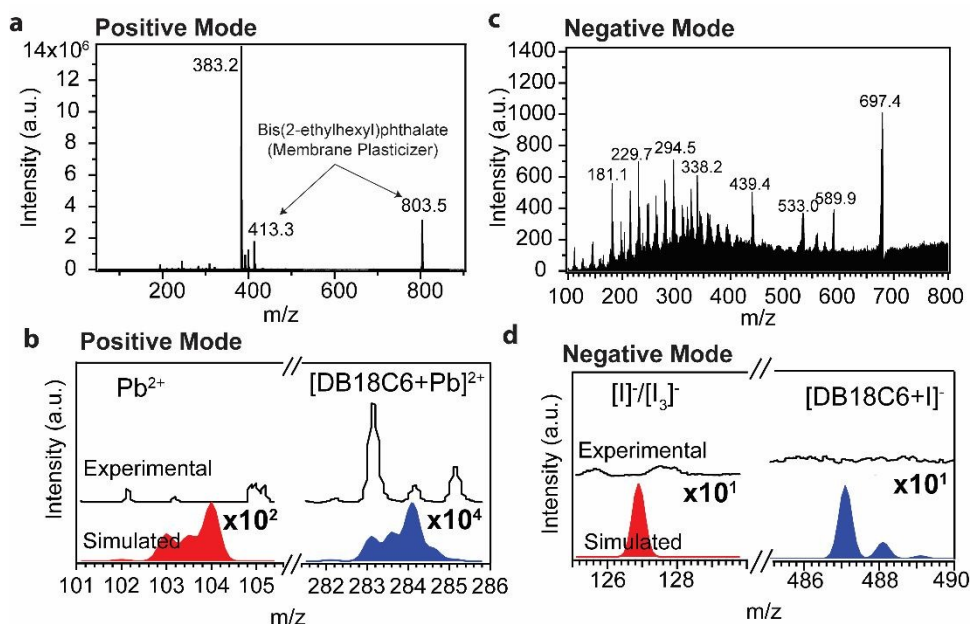


Figure 4. (a) Mass spectrum taken in positive mode of the membrane solution after the experiment from Figure 2a was run. (b) Zoomed in from (a) shows experimental (top) and simulated (bottom) spectra from the anticipated region of either bound or unbound Pb^{2+} . (c) Mass spectrum taken in negative mode of the membrane solution after experiment. (d) zoomed in from (c) shows experimental (top) and simulated (bottom) spectra from the anticipated region of either bound or unbound I^- .

We note that the purpose of these experiments was to impose harsh conditions on the sample for an extended period of time to determine which ions (if any) diffuse both within the HOIP and into the membranes. This is not to say that the timescale by which these characterization measurements were conducted (h) is comparable to the timescale which ion-transport is observed in HOIPs (ms). Given the fact that MA^+ was the only ion that was observed in the ISMs, it is reasonable to conclude that if Pb^{2+} , H^+ or I^- are mobile in HOIPs, then the ISM would present a blocking boundary for these ions, which should result in particular EIS features. In order to determine the EIS response of our ISMs given known anionic and cationic conduction, we conducted control experiments using (1) a positive control of poly(styrene sulfonate) sodium salt (PSS), where the anionic polymer backbone facilitates Na^+ conduction and (2) a negative control of poly(*N*-methyl-4-vinylpyridinium iodide), (PVPI) where the cationic polymer backbone facilitates I^- conduction (For structures, see Figures S3 and S10).

The EIS of pristine PSS and PVPI show features attributable to ionic conduction (Figure S9 and S10). Since our ISM is a cation-selective membrane, we expect a PSS-ISM interface to be a cation adsorbing interface and PVPI-ISM to be an anion blocking interface. The influence of these interfacial characteristics on mass diffusion impedance is well documented and can be qualitatively assessed based on the low-frequency response.¹³ Warburg mass diffusion typically manifests as a linear 45° region on the Nyquist plot, followed by either a curvature back into the real axis in the case of an absorbing boundary or, up to a vertical capacitive line in the case of a blocking boundary.²¹ In the case of PVPI, we saw a response characteristic of blocking consistent with the cationic selectivity of the ISM (Figure S9). In the positive control containing mobile Na^+ , we do not observe the same blocking

response (Figure S10). Interestingly, in the positive control, we do not observe a defined 45° linear region characteristic of Warburg ion diffusion. In the case of Warburg mass diffusion, a significant depression of the linear angle (as low as almost 0°) has been reported for systems in the case of absorbing boundary conditions, and in systems where diffusion of conducting particles is complicated by primary ion adsorption process.¹³ It is noteworthy that in the HOIP sample under illumination, we observed a response strikingly similar to our Na^+ conductive control, which indicates that the observed EIS response in our HOIP sample arises from mobile cations. However, we cannot conclusively rule out the presence of I^- below the detection limits of ESI-MS and EDX in these membranes. We therefore conclude that MA^+ is the primary ionic species within the ISMs during device measurements and we speculate that this ion is (at least in part) responsible for the observed EIS response.

Modeling the EIS response

The impedance response of HOIP samples sandwiched between ISM electrodes can be broken into three distinct sections; 1) a high-frequency semicircle, 2) a mid-frequency depressed linear region and, 3) a low-frequency capacitive response (Figure 5). To model this response, we turned to literature detailing EIS modeling of supercapacitor devices, where ions are incorporated into porous electrodes. We reasoned that these systems are similar to our devices. Therefore, we used a commonly utilized supercapacitor model²²⁻²⁴ as a scaffold to design our equivalent circuit (Figure S11). This model consists of a Warburg component, modeling ion diffusion to an absorbing boundary in the high to mid-frequency region, and a resistor and capacitor (or constant phase element) in parallel (*R-CPE*) in the low-frequency to model resistance and capacitance

associated with leakage of the capacitor. Ion diffusion is always associated with charge transfer resistance (R_{ct}) and double layer capacitance (C_{dl}). This literature model provides reasonable fits to our experimental data; however, the fit deviates in the high and mid-frequency region. Thus, to model our data we expanded the circuit to include an additional R - C component in the high-frequency range to account for bulk resistance and capacitance of the ISM. We reason that the ISM results in non-negligible impedance; therefore, it should be represented in our model. The resulting equivalent circuit is shown in Figure 5b. This model provides good fits to the data, as measured by the

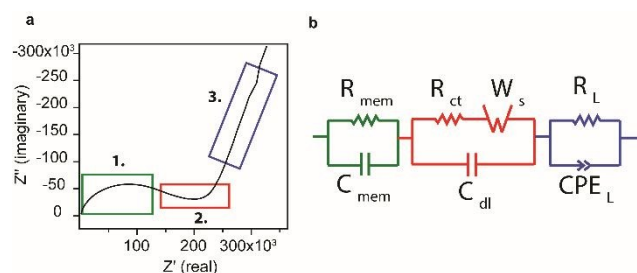


Figure 5. (a) The EIS response of the ISM device separated into high-frequency (1.) mid-frequency (2.) and low frequency (3.) response. (b) The proposed circuit model representing the EIS response. The high-frequency response is fit to an R - C circuit arising from membrane bulk capacitance, the mid-frequency region is fit with a Warburg element to capture ion diffusion, and the low frequency response is fit to another R - C modeling leaky capacitance arising from electronic or ionic accumulation.

low sum of squares and χ^2 values (Figure S11). We also considered the possibility that the low-frequency component may arise due to ion diffusion to a blocking boundary, which would be the case for MA^+ diffusion to the ITO interface, or I^- diffusion to the ISM interface. To test this, we modeled the system with no low-frequency R - CPE and, instead, modified the model with an open Warburg element to reflect blocking boundary conditions (Figure S11). However, this modified model did not fit the data as closely as the model from Figure 5b; thus, we assume that the low-frequency component is due to ion diffusion to an absorbing boundary. This is consistent with MA^+ diffusion to the ISM.

When we fit our data to the model in Figure 5b, the Warburg element modeling ion diffusion fits to a time constant on the order of ms (~ 10 ms), similar to what has been observed for mobile ions in thin-film photovoltaic devices. Considering the dimensions of the pellet and taking into account Warburg diffusion resistance, we estimate the ionic conductivity for the mobile ion to be on the order of 10^{-7} - 10^{-8} S cm^{-1} , which is also in the range of what we have observed for ions in thin-film devices.⁷

It is important to point out that there remains a significant debate regarding the nature of the mobile ion(s) in HOIP photovoltaics, specifically with regards to the timescale of MA^+ and I^- migration. It has been established that I^- is likely mobile under device operating conditions.²⁵⁻²⁷ However, there is less consensus on the timescale of migration for this ion. Some reports speculate ultrafast I^- migration occurs on the sub- μ s timescale ($< 1 \mu$ s)⁸ while others report I^- migration on a slow- μ s to fast-ms timescale.^{28, 29} For studies that have reported the migration of MA^+ , the timescale for migration is even more contested; timescales ranging from ms^{8, 30}, to μ s^{31, 32}, to > 1000 s³³

have been reported. In this work, we observe a response that is consistent with cation migration which fits to a ms time constant. We note that the data presented in this work is consistent with MA^+ . However, seeing that I^- conduction may also occur on the ms timescale, there is a possibility that this ion contributes to the EIS response of our system. At this point, we cannot comment on the contribution of anionic species since our ISMs were selective only to cations. A full validation of this model including the use of anionic selective membranes is the scope of our future work.

Importantly, the results from $MAPbI_3$ pellets with ISMs are consistent with observations in thin-film photovoltaic devices without ISMs. This is a promising result which demonstrates that this technique could be applied to selectively study ion migration in HOIP devices using EIS. We are currently in the process of placing ISMs on thin-film photovoltaic devices to study ion transport under device operating conditions and validating the equivalent circuit model through other experiments. We will report the results of these investigations in due course.

Conclusions

We have shown that placing cation selective ISMs between the sample and electrodes allows us to measure ion-selective EIS. We deployed this system to study ionic diffusion in HOIPs under illumination. With this device, we show evidence of an impedance arising from ionic conduction through the HOIP material. We show evidence that the ISMs are selective for MA^+ , confirming the mobility of this cation. Furthermore, the EIS response in our system fits to a ms time constant which suggests that MA^+ may be mobile on this timescale.

Conflicts of interest

There are no conflicts to declare.

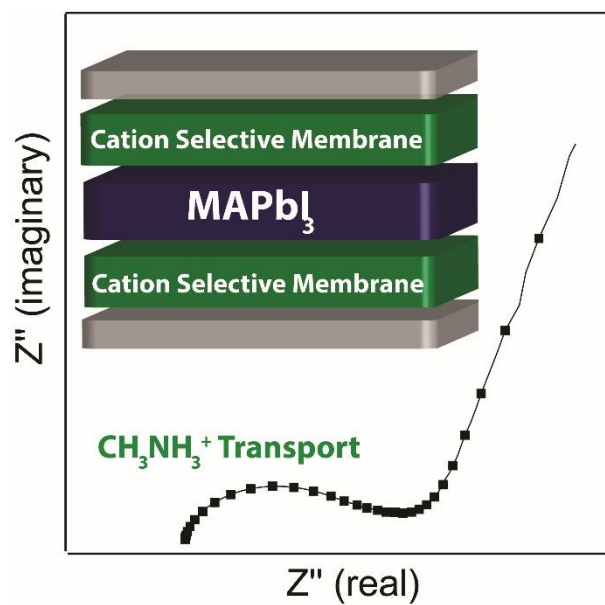
Acknowledgments

We gratefully acknowledge the financial support of Army Natick Soldier R D and E Center through contract no. W911QY1820002 for this work. The acquisition of the powder X-ray diffractometer was made possible through the National Science Foundation Major Research Instrumentation Program (CHE-1726578). We also thank Prof. Richard Vachet for his help with mass spectrometry. We gratefully acknowledge the helpful and insightful comments from the reviewers.

Notes and references

1. W. Tress, N. Marinova, T. Moehl, S. M. Zakeeruddin, M. K. Nazeeruddin and M. Gratzel, *Energy Environ. Sci.*, 2015, **8**, 995-1004.
2. S. Meloni, T. Moehl, W. Tress, M. Franckevicius, M. Saliba, Y. H. Lee, P. Gao, M. K. Nazeeruddin, S. M. Zakeeruddin, U. Rothlisberger and M. Graetzel, *Nat. Commun.*, 2016, **7**, 9.

3. G. Richardson, S. E. J. O'Kane, R. G. Niemann, T. A. Peltola, J. M. Foster, P. J. Cameron and A. B. Walker, *Energy Environ. Sci.*, 2016, **9**, 1476-1485.
4. I. Levine, P. K. Nayak, J. T. W. Wang, N. Sakai, S. Van Reenen, T. M. Brenner, S. Mukhopadhyay, H. J. Snaith, G. Hodes and D. Cahen, *J. Phys. Chem. C*, 2016, **120**, 16399-16411.
5. S. van Reenen, M. Kemerink and H. J. Snaith, *J. Phys. Chem. Lett.*, 2015, **6**, 3808-3814.
6. C. Eames, J. M. Frost, P. R. F. Barnes, B. C. O'Regan, A. Walsh and M. S. Islam, *Nat. Commun.*, 2015, **6**, 8.
7. J. Haruyama, K. Sodeyama, L. Y. Han and Y. Tateyama, *J. Am. Chem. Soc.*, 2015, **137**, 10048-10051.
8. J. M. Azpiroz, E. Mosconi, J. Bisquert and F. De Angelis, *Energy Environ. Sci.*, 2015, **8**, 2118-2127.
9. A. Pockett, G. E. Eperon, N. Sakai, H. J. Snaith, L. M. Peter and P. J. Cameron, *Phys. Chem. Chem. Phys.*, 2017, **19**, 5959-5970.
10. M. N. F. Hoque, N. Islam, Z. Li, G. F. Ren, K. Zhu and Z. Y. Fan, *ChemSusChem*, 2016, **9**, 2692-2698.
11. E. C. Smith, C. L. C. Ellis, H. Javaid, L. A. Renna, Y. Liu, T. P. Russell, M. Bag and D. Venkataraman, *J. Phys. Chem. C*, 2018, **122**, 13986-13994.
12. D. Pitarch-Tena, T. T. Ngo, M. Valles-Pelarda, T. Pauporte and I. Mora-Sero, *ACS Energy Lett.*, 2018, **3**, 1044-1048.
13. V. F. Lovich, *Impedance Spectroscopy: Applications to Electrochemical and Dielectric Phenomena*, John Wiley & Sons, Inc., Hoboken, New Jersey, 2012.
14. T. Katsu and M. Matsumoto, *Anal. Sci.*, 2001, **17**, 721-725.
15. T. Katsu and N. Nishimura, *Anal. Sci.*, 2000, **16**, 523-525.
16. T. Katsu, D. F. Xu, K. Tsuji and T. Nagamatsu, *Anal. Chim. Acta*, 1997, **354**, 301-305.
17. M. A. Akl and M. H. Abd El-Aziz, *Arab. J. Chem.*, 2016, **9**, S878-S888.
18. M. O'Rourke, N. Duffy, R. D. Marco and I. Potter, *Membranes*, 2011, **1**, 132-148.
19. M. S. Yin, F. X. Xie, H. Chen, X. D. Yang, F. Ye, E. B. Bi, Y. Z. Wu, M. T. Cai and L. Y. Han, *J. Mater. Chem. A*, 2016, **4**, 8548-8553.
20. R. M. Izatt, K. Pawlak, J. S. Bradshaw and R. L. Bruening, *Chem. Rev.*, 1991, **91**, 1721-2085.
21. J. Landesfeind, D. Pritzl and H. A. Gasteiger, *J. Electrochem. Soc.*, 2017, **164**, A1773-A1783.
22. W. Wang, S. R. Guo, I. Lee, K. Ahmed, J. B. Zhong, Z. Favours, F. Zaera, M. Ozkan and C. S. Ozkan, *Sci Rep*, 2014, **4**, 9.
23. C. Masarapu, H. F. Zeng, K. H. Hung and B. Q. Wei, *ACS Nano*, 2009, **3**, 2199-2206.
24. R. S. Hastak, P. Sivaraman, D. D. Potphode, K. Shashidhara and A. B. Samui, *Electrochim. Acta*, 2012, **59**, 296-303.
25. D. W. Dequillettes, W. Zhang, V. M. Burlakov, D. J. Graham, T. Leijtens, A. Osherov, V. Bulovic, H. J. Snaith, D. S. Ginger and S. D. Stranks, *Nat. Commun.*, 2016, **7**, 9.
26. A. Senocrate, I. Moudrakovski, G. Y. Kim, T. Y. Yang, G. Gregori, M. Gratzel and J. Maier, *Angew. Chem.-Int. Edit.*, 2017, **56**, 7755-7759.
27. T. Y. Yang, G. Gregori, N. Pellet, M. Gratzel and J. Maier, *Angew. Chem.-Int. Edit.*, 2015, **54**, 7905-7910.
28. S. A. L. Weber, I. M. Hermes, S. H. Turren-Cruz, C. Gort, V. W. Bergmann, L. Gilson, A. Hagfeldt, M. Graetzel, W. Tress and R. Berger, *Energy Environ. Sci.*, 2018, **11**, 2404-2413.
29. C. Li, A. Guerrero, S. Huettner and J. Bisquert, *Nat. Commun.*, 2018, **9**, 8.
30. M. Bag, L. A. Renna, R. Y. Adhikari, S. Karak, F. Liu, P. M. Lahti, T. P. Russell, M. T. Tuominen and D. Venkataraman, *J. Am. Chem. Soc.*, 2015, **137**, 13130-13137.
31. Y. B. Yuan, J. Chae, Y. C. Shao, Q. Wang, Z. G. Xiao, A. Centrone and J. S. Huang, *Adv. Energy Mater.*, 2015, **5**, 7.
32. M. H. Futscher, J. M. Lee, L. McGovern, L. A. Muscarella, T. Wang, M. I. Haider, A. Fakharuddin, L. Schmidt-Mende and B. Ehrler, *Materials Horizons*, 2019.
33. K. Domanski, B. Roose, T. Matsui, M. Saliba, S. H. Turren-Cruz, J. P. Correa-Baena, C. Roldan-Carmona, G. Richardson, J. M. Foster, F. De Angelis, J. M. Ball, A. Petrozza, N. Mine, M. K. Nazeeruddin, W. Tress, M. Gratzel, U. Steiner, A. Hagfeldt and A. Abate, *Energy Environ. Sci.*, 2017, **10**, 604-613.



Using Ion-selective impedance spectroscopy to study cation transport in hybrid organic-inorganic perovskites.